PNAS RESEARCH ARTICLE | BIOCHEMISTRY CHEMISTRY

Biocatalytic control of site-selectivity and chain length-selectivity in radical amino acid halogenases

Elijah N. Kissman[a,1], Monica E. Neugebauer[b,1], Kiera H. Sumida[a], Cameron V. Swenson[a], Nicholas A. Sambold[c], Jorge A. Marchand[b], Douglas C. Millar[b], and Michelle C. Y. Chang[a,b,c,2]

Edited by Hans Renata, Rice University, Houston, TX; received August 25, 2022; accepted February 14, 2023 by Editorial Board Member Stephen J. Benkovic

Biocatalytic C–H activation has the potential to merge enzymatic and synthetic strategies for bond formation. Fe^{II}/αKG-dependent halogenases are particularly distinguished for their ability both to control selective C–H activation as well as to direct group transfer of a bound anion along a reaction axis separate from oxygen rebound, enabling the development of new transformations. In this context, we elucidate the basis for the selectivity of enzymes that perform selective halogenation to yield 4-Cl-lysine (BesD), 5-Cl-lysine (HalB), and 4-Cl-ornithine (HalD), allowing us to probe how site-selectivity and chain length selectivity are achieved. We now report the crystal structure of the HalB and HalD, revealing the key role of the substrate-binding lid in positioning the substrate for C_4 vs C_5 chlorination and recognition of lysine vs ornithine. Targeted engineering of the substrate-binding lid further demonstrates that these selectivities can be altered or switched, showcasing the potential to develop halogenases for biocatalytic applications.

biocatalysis | enzymology | bioinorganic chemistry | structural biology | C-H activation

Significance

Selective C–H bond activation is a challenging transformation critical to the synthesis of pharmaceuticals and fine chemicals. A recently identified family of radical halogenases accomplishes site-selective C–H activation of amino acids followed by chlorination, bromination, or azidation. We compare the crystal structures of three halogenases which produce 4-Cl-lysine, 5-Cl-lysine, and 4-Cl-ornithine to identify a substrate-binding lid region in the highly variable C terminus. These structures reveal a striking difference in substrate conformation leading to divergent outcomes. Engineering of key residues alters the substrate and site-selectivity of HalB and HalD and further illustrates the significance of the C terminus in determining selectivity. This work deepens our understanding of site-selective C–H activation and will enable further efforts in enzyme engineering for synthetic applications.

The use of enzymes as biocatalysts has expanded the scope of chemical synthesis by introducing new avenues for reducing synthetic steps to minimize waste and cost for industrial synthesis (1–4). Given their potential for high selectivity and compatibility with mild aqueous conditions compared to chemical catalysts, the integration of enzymes with traditional synthetic chemistry has changed the landscape of what can be achieved by telescoped and single-pot synthetic routes (5–7). While several classes of enzymes, such as ketoreductases, transaminases, hydrolases, and lyases, can be reliably incorporated into commercial synthesis (8), there remains a need for new reaction classes in order to blend biological and chemical catalysis. In this regard, selective C–H activation and functionalization could enable new C–C bond-forming connections to rapidly assemble complex molecules by interfacing enzymatic selectivity for C–H activation with the breadth of downstream synthetic reactions used for bond making and cross-coupling (Fig. 1*A*).

Although C–H activation reactions have found high utility in synthetic chemistry, site selectivity can be challenging to achieve as the weakest or most sterically accessible C–H bond is typically activated by the catalyst, it can be difficult to prevent undesired activation of C–H bonds of similar strength, and functional group compatibility can be low (9). To address these challenges, chemical catalysts have been designed to use ligand architecture or spatial orientation to achieve selectivity (10–16). In contrast, enzymes routinely achieve both stereo- and site-selectivity when presented with similar sites of equivalent reactivity since their three-dimensional chiral architecture naturally creates asymmetry. Although the most common outcome for enzymatic C–H activation is O atom transfer, enzymes have been harnessed for myriad useful reactions including C–C bond formation (17, 18), amination (19), azidation (20), silation (21), and borylation (22). Thus, C–H activating enzymes provide a promising starting point for diversifying and expanding the role of biocatalysis in chemistry.

Many classes of metalloenzymes, including cytochrome P450s (23, 24), Fe/αKG-dependent enzymes (25–30), and Rieske enzymes (31, 32) have been used for biocatalytic C–H activation reactions via H atom abstraction to form a substrate radical intermediate. Radical-based transformations have particularly stringent requirements for active-site geometry; not only is there a strong distance dependence for hydrogen atom abstraction, but the reactive nature of the intermediates can lead to a wide range of side reactions if not precisely coordinated (33). We are particularly interested in studying Fe/αKG-dependent halogenases as a paradigm for understanding the geometric active-site constraints that control site and reaction selectivity for C–H activation and rebound. In Fe/αKG-dependent halogenases, substrate radical formation by a ferryl intermediate and subsequent substrate radical functionalization with halide (X = Cl, Br) occur along different vectorial

Author contributions: E.N.K., M.E.N., K.H.S., C.V.S., N.A.S., J.A.M., D.C.M., and M.C.Y.C. designed research; E.N.K., M.E.N., K.H.S., C.V.S., N.A.S., J.A.M., and D.C.M. performed research; E.N.K., M.E.N., K.H.S., C.V.S., N.A.S., J.A.M., D.C.M., and M.C.Y.C. analyzed data; and E.N.K., M.E.N., and M.C.Y.C. wrote the paper.

The authors declare no competing interest.

This article is a PNAS Direct Submission. H.R. is a guest editor invited by the Editorial Board.

[1]E.N.K. and M.E.N. contributed equally to this work.

[2]To whom correspondence may be addressed. Email: mcchang@berkeley.edu.

This article contains supporting information online at https://www.pnas.org/lookup/suppl/doi:10.1073/pnas.2214512120/-/DCSupplemental.

Published March 13, 2023.

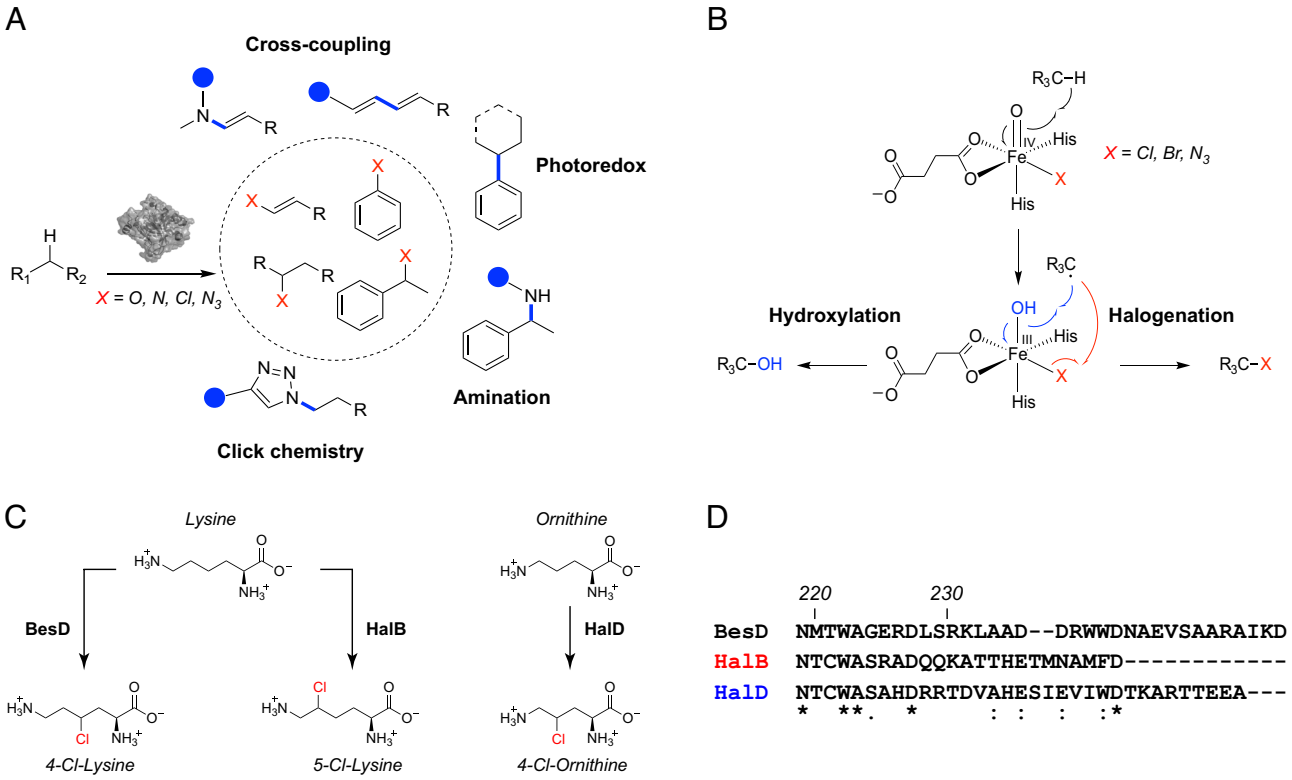

Fig. 1. Radical amino acid halogenases as biocatalysts. (*A*) Enzymatic C–H activation has been utilized for selective C–C and C-heteroatom bond formation. These products have been combined with downstream synthetic and enzymatic reactions to form pharmaceutically relevant intermediates. (*B*) Control of the reactive Fe^{IV}-oxo intermediate can enable the delivery of alternate anions such as azide. Engineering the enzymes while avoiding off-pathway hydroxylation has been an ongoing challenge. (*C*) Site-selectivity of lysine halogenases. BesD chlorinates lysine at C_4 to yield 4-Cl-lysine. HalB chlorinates lysine at C_5 to yield 5-Cl-lysine. HalD displays substrate selectivity for ornithine, which is one carbon shorter than lysine. (*D*) The C terminus of the halogenases varies significantly depending on the substrate- and site-selectivity. HalB and HalD align more closely while BesD is longer and shares fewer similar residues. The annotated C-terminal region is shown in bold, and residue numbering is based on the sequence of BesD.

paths (Fig. 1*B*) (34–38). This behavior leads to flexibility in transferring new and abiotic anions, such as azide (20), but also presents challenges for active site engineering.

Biocatalytic applications of Fe-/αKG-dependent halogenases have been limited by the relatively small number of halogenases discovered to date as well as the difficulty in engineering their substrate selectivity without altering their reaction pathway towards hydroxylation. The first reported radical halogenase family was found to require a carrier-protein tethered substrate (39–46). However, new families of radical halogenases have been discovered to act on freestanding substrates, including alkaloids (47), nucleotides (48), and amino acids (49). These families collectively provide promising new scaffolds for diversification in both substrate and reaction range (30, 50). We discovered a new family of Fe^{II}/αKG-dependent halogenases (BesD) that carries out the site-selective and stereoselective C(sp^3)-H activation of simple amino acid substrates without the need for a carrier protein (51). Given the privileged role of amino acids as building blocks for biosynthesis, catalyst design, and drug discovery (52), elucidation of the sequence and structural determinants that govern the substrate selectivity of BesD halogenases can allow us to tap their potential use in biocatalytic applications.

Toward this goal, we investigate enzymes within the BesD amino acid halogenase family that perform subtly different reactions to selectively yield either 4-chlorolysine (BesD), 5-chlorolysine (HalB), or 4-chloroornithine (HalD) (Fig. 1*C*). Through bioinformatics analysis and X-ray crystallography of HalB, we identify a C-terminal substrate-binding lid that undergoes an unprecedented conformational change to control site-selectivity and substrate-selectivity within this family. To understand how BesD and HalB chlorinate lysine at C_4 and C_5, respectively, we solve the lysine-bound crystal structure of HalB for comparison to BesD (51), which reveals how structurally distinct substrate-binding lids tune the substrate conformation within the active site to achieve divergent selectivity. Through site-directed mutagenesis and fluorogenic screening, we identify mutations that disrupt site-selectivity and support the proposed role of the substrate-binding lid in controlling reactivity. Next, we solve the crystal structure of the ornithine halogenase, HalD, which has a 40-fold lower K_M for the 5-carbon substrate, ornithine, compared to the 6-carbon substrate, lysine. The ornithine and lysine halogenases are structurally similar except at the lid domain, which closes over the substrate in the active site. Structure-guided engineering of the HalD lid expands the substrate binding pocket, enabling HalD to chlorinate lysine with a K_M comparable to that of HalB. Taken together, this work provides fundamental insights into the basis of site-selective halogenation of unactivated C_{sp3}–H bonds and suggests that the substrate binding lid may be a promising engineering target for future efforts to tailor radical halogenases for the biocatalytic chlorination of a broad range of substrates.

Results

Amino Acid Halogenases Have Variable C-Termini Which Are Involved in Substrate Binding. Given the synthetic utility of reactions catalyzed by Fe/αKG-dependent enzymes and halogenation in particular, a detailed understanding of how these enzymes recognize small molecule substrates is key to expanding their biocatalytic applications. Indeed, the substrate selectivities

found within the BesD radical halogenase family allow us to explore the molecular basis for how site-selectivity and chain length selectivity is controlled (Fig. 1*C*) (51). We previously solved the crystal structure of the lysine 4-chlorinase, BesD, which shows that the C-terminal domain (residues 229 to 252) forms a lid over the substrate in the active site (51). This closed active site appears to be conserved in other structures of Fe/αKG-dependent enzymes and in some other radical-utilizing enzymes that accept small molecule rather than protein-bound substrates (53). Interestingly, a sequence alignment of BesD (4-chlorolysine), HalB (5-chlorolysine), and HalD (4-chloroornithine), revealed that the active-site residues are highly conserved except those within the C-terminal lid, which varies in length and sequence (Fig. 1*D* and *SI Appendix,* Fig. S1). Given the role of the C-terminal domain in forming the active site and its variability, we decided to further explore its role in substrate selectivity.

Toward this end, we initiated structural studies of HalB, which chlorinates the same lysine substrate as BesD but at C_5 instead of C_4 (51). Notably, the HalB C terminus (15 amino acids) is 40% shorter than that of BesD (25 amino acids) and the two C-terminal sequences align poorly. HalB crystals formed in succinate-phosphate-glycine buffer, diffracted to 2.05 Å, and contained two copies of HalB per asymmetric unit (*SI Appendix*, Table S2). Strikingly, the two copies of HalB adopted surprisingly different conformations depending on the presence or absence of a bound amino acid. In the apo chain A, no amino acid is found in the active site and the C-terminal domain (residues 238 to 251) that forms the substrate lid is disordered (Fig. 2*C*). In chain B, density for glycine is present in the enzyme active site in the position expected for the substrate lysine, likely due to the high concentration of glycine in the crystallization conditions (21.8 mM) (Fig. 2 *A* and *B*). In the presence of an amino acid, the C-terminal domain becomes structured. In the absence of an amino acid, the antiparallel beta strands (residues 68 to 88) that bind the carboxylate of the substrate via Arg83 are instead projected away from the active site to adopt an extended alpha-helical structure. Although substrate-covering lids have been identified in other Fe/αKG-dependent enzymes (36, 53), the observed helix-to-sheet transition is unique to HalB. This snapshot of HalB in two different states suggests that HalB undergoes a conformational change upon substrate binding with the C-terminal lid forming part of the active site to participate in substrate recognition and catalysis.

Lysine-Bound Crystal Structure of HalB. To investigate how the C-terminal lid of HalB interacts with its native substrate, we next solved the lysine-bound structure of HalB to 1.90 Å by screening for crystal formation in conditions containing lysine instead of glycine (*SI Appendix,* Table S3). Under the new crystallization conditions, density for the lysine ligand is clearly visible in the active site of HalB (Fig. 3*A*). The structures of HalB and BesD are similar except at their C-terminal lids, which close over the substrate in the active site (Fig. 3*B*). While the C terminus of BesD is longer and lacks secondary structure, the C terminus of HalB is shorter and α-helical. An overlay of the crystal structures of HalB and BesD reveals that the enzymes have conserved carboxylate and α-amine binding residues (Fig. 3*C*). As a result, the lysine substrate is located in a similar position in the active site and is not translationally shifted in HalB compared to BesD. However, we observed striking differences in the conformation of lysine within the active sites. In BesD, C_4 of lysine is oriented toward the Fe complex. In contrast, C_5 of lysine is instead presented toward the complex in HalB, while C_4 is pointed away. The conformations of lysine within each structure are consistent with the observed selectivity of the two enzymes (Fig. 2*C*). In addition, HalB and BesD demonstrate the same prochiral behavior, with the pro-*R* hydrogen presented toward the Fe complex for hydrogen atom abstraction (*SI Appendix,* Figs. S2 and S3).

Notably, the key residues that contribute to the conformational differences of lysine are located on the C-terminal substrate-binding lids. In BesD, Trp239 stacks against the aliphatic side chain of lysine in the active site. In HalB, this Trp residue is absent. Instead, Met246 protrudes into the active site and presents C_5 of lysine toward the Fe complex, making it accessible for halogenation. Thus, Met246 makes a steric contribution to halogenation of lysine at C_5. This mechanism is distinct from some other amino-acid modifying enzymes which enforce site-selectivity by translationally shifting the substrate. For example, lysine 3-hydroxylase KDO1 binds the substrate carboxylate with Arg332 while lysine 4-hydroxylase KDO5 pulls the substrate farther into the active site to interact with Arg145 which is absent in KDO1 (53). In comparison, while lysine adopts an altered conformation in the active site of BesD and HalB (all-atom root-mean-square deviation (RMSD) 1.112 Å), there is no significant shifting of the key binding determinants, with the α-carboxylate, α-amine, and ε-amine shifted by just 0.2, 0.4, and 0.6 Å, respectively.

In addition to substrate selectivity controlled by hydrogen atom abstraction, radical halogenases also need to solve the challenge of rebound selectivity in the next step with the halide ligand over the thermodynamically preferred pathway of hydroxyl ligand rebound (*SI Appendix,* Fig. S4) (29, 54). The selectivity of rebound has been hypothesized to be derived from precise control over the substrate radical positioning relative to the two potential rebounding species

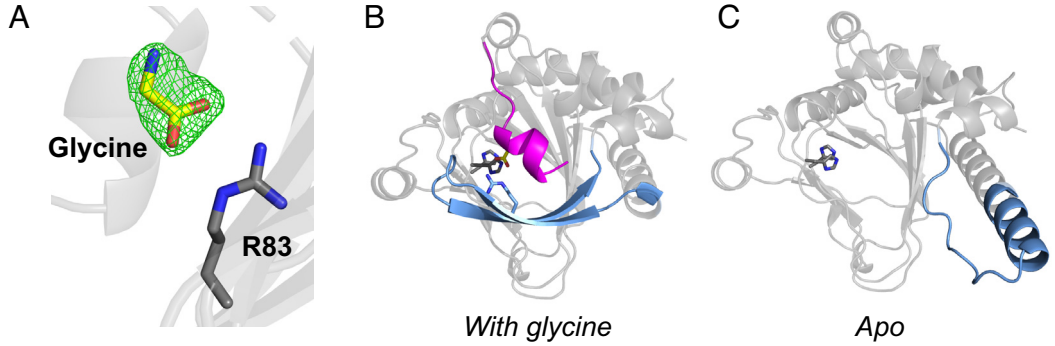

Fig. 2. HalB undergoes a conformational change upon substrate binding. (*A*) Crystal structure of glycine-bound Chain A of HalB (2.05 Å) with F_o-F_c omit map (green mesh contoured at 1.5 σ) for glycine (yellow). (*B*) Structure of glycine-bound HalB with the C-terminal domain (residues 238 to 251) shown in magenta and the antiparallel beta strands containing Arg83 shown in blue (residues 68 to 88). (*C*) Structure of apo chain A of HalB with the alpha-helical domain in blue. The residues in the alpha-helical domain correspond to the residues in the beta strands in (*B*). The C-terminal domain (residues 238 to 251) is disordered and therefore not modeled.

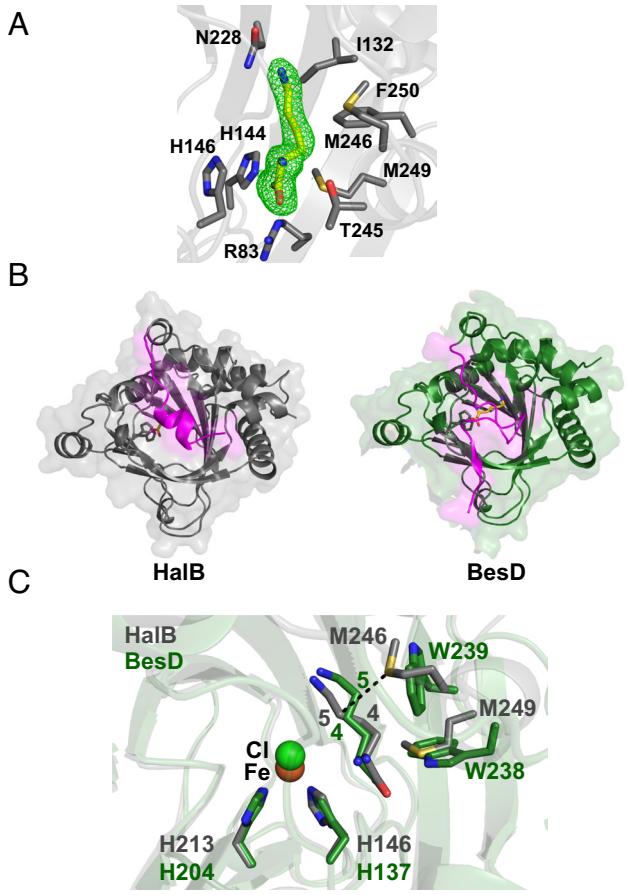

Fig. 3. Structural basis of site-selectivity. (*A*) Crystal structure of HalB (1.9 Å) with F_o-F_c omit map (green mesh, contoured at 1 σ) for lysine (yellow). Active site residues of HalB are shown as gray sticks. (*B*) Comparison of the overall structures of HalB (1.90 Å, gray) and BesD (1.95 Å, green, PDB 6NIE). The enzymes share high structural similarity except at the substrate covering lid (magenta). (*C*) Structural alignment of HalB (gray) and BesD (green). Although the carboxylate and amine of lysine are in a similar position in both cases, the sidechain samples a different conformation in the two enzymes. In BesD, C_4 is oriented toward chloride in the active site, while C_5 is oriented away. In contrast, HalB orients C_5 toward chloride. The substrate conformation is influenced by residues in the substrate covering lids of BesD and HalB. In particular, Met246 in HalB makes a steric contribution to the reaction outcome.

to allow for the more difficult halogenation reaction to occur (34–37, 55, 56). Although pairs of Fe^{II}/αKG-dependent amino acid hydroxylases with regio-divergent outcomes have been reported (53, 57–59), it is remarkable that the two halogenases, BesD and HalB, overcome the additional challenge of precisely orienting lysine within the active site to achieve site-selectivity without compromising the selectivity for halogenation over hydroxylation.

Investigating the Role of Met246. To probe the significance of Met246 on the selectivity of HalB, we generated a M246 NNK site-saturation library to determine whether mutagenesis could perturb the site-selectivity of HalB for modifying C_5 and result in chlorination of C_4 as well. To assay the variants, we employed a fluorogenic screen (60) based on the role of 4-Cl-lysine as an intermediate in the biosynthesis of propargylglycine (Pra), a terminal-alkyne containing amino acid (Fig. 4*A*) (49). In this pathway, 4-Cl-lysine produced by BesD is a substrate for the downstream enzymes BesC and BesB, which form Pra (49). If lysine is chlorinated at C_5 instead, Pra is not formed, since 5-Cl-lysine is not a substrate for BesC and BesB. As a result, only cells that produce 4-Cl-lysine enable copper-catalyzed azide-alkyne cycloaddition (CuAAC) with the fluorogenic probe CalFluor 488 (*SI Appendix,* Fig. S5) (61). This screen can therefore be used to determine whether mutagenesis of Met246 in HalB disrupts site-selective halogenation of C_5.

We transformed the HalB M246 NNK library into cells containing *besC* and *besB* and inoculated 168 colonies into a 96-well plate. The library was screened for alkyne formation alongside wild-type BesD, HalB, and Hydrox, a negative control which makes 4-hydroxylysine (60). After 4 d of expression, the cells were removed by centrifugation, and the supernatants were analyzed by CuAAC with CalFluor 488 (*SI Appendix,* Fig. S6). As expected, cells expressing HalB (lysine 5-halogenase) yielded no fluorescence increase relative to the negative control, consistent with the lack of 4-Cl-lysine production. In contrast, cells expressing BesD (lysine 4-halogenase) yielded an eightfold increase in fluorescence. The screen identified 26 variants among the NNK library that yielded a twofold increase in fluorescence intensity relative to Hydrox (*SI Appendix,* Fig. S6). Plasmids from these alkyne-producing cells were isolated and sequenced to identify mutations that enabled 4-Cl-lysine formation. M246L, M246I, M246V, and M246T appeared among the 26 sequenced hits (*SI Appendix,* Table S4). The results suggest that replacement of Met246 with smaller and/or nonpolar residues may alleviate steric constraints that position C_5 close to the catalytic Fe, thereby enabling chlorination of C_4 as well.

Characterization of HalB Variants. We repeated the assay with replicates of each of these clones and determined that M246V, M246L, M246I, and M246T yielded a fourfold, 2.75-fold, 2.5-fold, and 1.67-fold fluorescence increase, respectively, relative to HalB (Fig. 4*B*). We selected the HalB mutants with the greatest signal from the click screen (HalB M246V, HalB M246L, and HalB M246I) for further characterization. We first evaluated the extent to which the mutations perturbed site-selectivity by comparing the amount of Pra produced in each condition (*SI Appendix,* Fig. S7). The lysine 4-halogenase, BesD, produced 6.1 ± 0.7 μM Pra in the spent media. HalB M246V resulted in the greatest Pra production, yielding 1.5 ± 0.4 μM Pra. The M246I and M246L mutants produced 0.7 ± 0.1 μM and 0.5 ± 0.1 μM Pra, respectively. The data suggest that M246 is important for site-selectivity and that mutagenesis of this residue leads to aberrant activation of C_4, albeit at levels much lower than observed in the native lysine 4-halogenase.

We next investigated whether the mutations that enabled C_4 chlorination might also lead to diminished overall activity. We purified HalB M246V, HalB M246L, and HalB M246I and performed steady-state kinetic analysis using an assay that couples succinate formation by the halogenase to nicotinamide adenine dinucleotide (NADH) oxidation (62). We found that all three mutants had a decreased k_{cat} and K_M relative to the wild type HalB enzyme, consistent with a perturbation of lysine binding in the enzyme active site (*SI Appendix,* Fig. S8). These kinetic data were consistent with mass spectrometry data showing that the M246 mutants exhibited as much as a twofold decrease in production of 5-chlorolysine compared to HalB (*SI Appendix,* Fig. S9). Given that active site mutations can reduce the selectivity for chlorination over hydroxylation, we also quantified the relative amounts of chlorolysine and hydroxylysine produced by the HalB variants. We observed a decrease in hydroxylation corresponding to the decrease in activity demonstrated by the kinetic data, suggesting that mutation of this position avoids reduced reaction selectivity (*SI Appendix,* Fig. S9). The promiscuity of the HalB variants supports the significance of the substrate binding pocket in influencing the substrate conformation and the resulting selectivity in BesD and HalB.

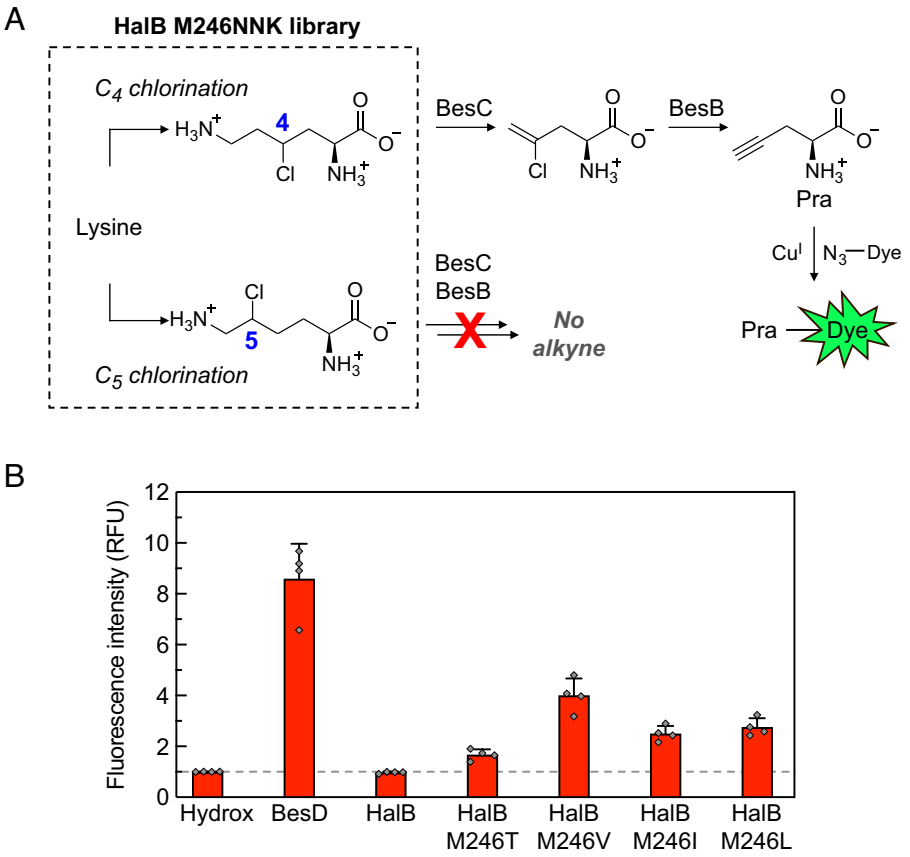

Fig. 4. Screening the HalB library for perturbation in site-selectivity. (*A*) Strategy for screening the M246NNK library for variants that perform halogenation. In two enzymatic steps, 4-Cl-lysine can be converted into Pra, which contains an alkyne functional group that can be leveraged for CuAAC chemistry with a fluorogenic probe. Variants that only perform chlorination of C_5 yield no fluorescence, as 5-Cl-lysine is not a substrate for the enzymes in the alkyne biosynthesis pathway. (*B*) Cells expressing a lysine 4-hydroxylase (Hydrox), lysine 4-halogenase (BesD), lysine 5-halogenase (HalB), or a variant of HalB, along with downstream enzymes BesB and BesC were grown in 96-well plates at 16 °C for 48 h, at which time the cultures were supplemented with lysine and αKG. After an additional 2 d of growth, cells were pelleted by centrifugation and the supernatant was analyzed for Pra by reaction with CalFluor 488, BTTAA, sodium ascorbate, and copper (II) sulfate. Following incubation in the dark for 15 min, fluorescence intensity was measured at room temperature (λ_{ex} = 485 nm, λ_{em} = 528 nm). Mean and SE are shown for n = 4 technical replicates.

We revisited the HalB crystal structure to determine whether additional residues may directly contribute to the observed site-selectivity. Phe250 in HalB is positioned 4.1 Å away from C_4 and forms a pocket which stabilizes C_4 away from the active site (Fig. 3*A*). To investigate the role of Phe250 on site-selectivity, we generated four separate NNK libraries at position 250 while keeping residue 246 constant as Met (wild type), Leu, Ile, or Val, the three mutations which yielded the greatest fluorescence in the screen. We screened over 150 colonies from each library using CuAAC (*SI Appendix,* Figs. S10–S13). However, none of the mutations at Phe250 led to significantly increased yield of 4-chlorolysine beyond the original M246I, M246L, M246V point mutants (*SI Appendix,* Tables S5–S7). These results suggest that point mutations are insufficient for fully altering site-selectivity, supporting the evolutionary logic of extensively remodeling the C-terminal lid of BesD and HalB to achieve divergent outcomes.

Crystal Structure of Ornithine Halogenase HalD. In addition to members that make distinct regio-isomers of chlorolysine, the BesD amino acid halogenase family also contains members that display substrate selectivity. The enzyme HalD selectively chlorinates ornithine (k_{cat}/K_M = 330 ± 70 $mM^{-1}min^{-1}$) over lysine (k_{cat}/K_M = 13.2 ± 3.6 $mM^{-1}min^{-1}$) (51). Interestingly, the two substrates only differ by one carbon. In HalD, the K_M for ornithine is 30 μM, which is within the range of intracellular ornithine concentrations (63). In contrast, the lysine 4-halogenase HalA, a homolog that performs the same reaction as BesD, has a K_M for ornithine of 160 μM, which is well above the expected concentration of ornithine in the cell (63). Although HalD chlorinates lysine and ornithine, the K_M value for lysine is 40 times higher (1.22 ± 0.12 mM vs 0.03 ± 0.004 mM), indicating a strong preference for ornithine (51).

We initiated comparative structural studies to understand how HalD exhibits chain-length preference for the shorter ornithine substrate. We co-crystallized HalD with ornithine and solved the structure to 2.0 Å (*SI Appendix,* Table S8). The structure possessed clear electron density for the ornithine substrate within the active site (Fig. 5*A*). We also observed density for chloride, αKG, and a metal between the Fe-binding His149 and His217 residues. Although iron is the catalytically-relevant metal, we assign the density in the structure as nickel based on our crystallography conditions and precedent for the persistence of nickel during nickel-affinity chromatography of Fe^{II}/αKG-dependent enzymes (64).

We next performed a structural comparison of HalD (ornithine 4-halogenase), BesD (lysine 4-halogenase), and HalB (lysine 5-halogenase). The cores of all three enzymes are structurally similar, and the substrates bind in a similar location in all three cases. Consistent with our proposed role of the C-terminal lid in dictating selectivity, the majority of the structural differences between the three enzymes occur within the C-termini (Fig. 5*B* and *SI Appendix,* Fig. S14). The C-terminal lid of the HalD aligns better with that of HalB (RMSD of 0.357 Å) than BesD (RMSD of 2.318 Å) (*SI Appendix,* Fig. S15). The lids of both HalD and HalB are alpha-helical in structure, while the C terminus of BesD lacks

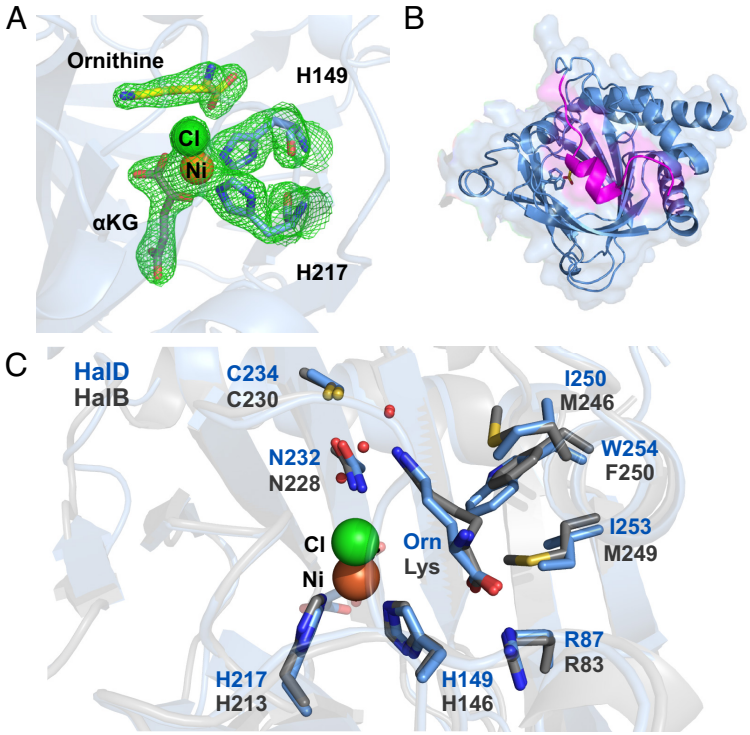

Fig. 5. Structural basis of chain length selectivity. (*A*) Density for ornithine in the active site of HalD (2.0 Å). F_o-F_c omit map (green mesh, contoured at 1.5 σ) for ornithine. (*B*) Overall fold of the ornithine halogenase, HalD. The substrate covering lid is shown in magenta. (*C*) Structural alignment of HalB (1.9 Å, gray) and HalD (2.0 Å, blue). In contrast to lysine in HalB, the ornithine substrate of HalD is present in an extended conformation, with C_4 poised for chlorination. HalD is unable to accommodate lysine in the active site because of steric strain imposed primarily by the substitution of Trp254 in place of phenylalanine.

secondary structure. Due to the high structural similarity of HalD and HalB, and because previous liquid chromatography-mass spectrometry (LC/MS) results suggest that HalD produces 5-Cl-lysine rather than 4-Cl-lysine (51), we chose HalB as the primary point of comparison for chain-length specificity.

A direct comparison of HalB and HalD revealed that the carboxylates and amines of lysine and ornithine are in very similar positions in the active site (shifted by 0.4, 0.3, and 0.5 Å for the α-carboxylate, α-amine, and ε-amine, Fig. 5*C*). However, while ornithine is bound in an extended conformation, the side chain of lysine is instead kinked away from the location of the catalytic Fe, making hydrophobic contacts with a binding pocket provided by the C-terminal covering lid. In the lysine halogenase, HalB, the substrate binding pocket is composed of Met246, Met249, and Phe250, which accommodate C_3 and C_4 of lysine (Fig. 6*A*). In contrast, the ornithine halogenase has a smaller pocket that is composed of Ile250, Ile253, and Trp254 (Fig. 6*B*). Notably, Trp254 in HalD is larger than Phe250 in HalB. As a result, the longer side chain of lysine is not readily accommodated in the HalD active site, consistent with the strong preference of HalD for ornithine.

Engineering the HalD Binding Pocket to Accommodate Lysine. Although HalB and HalD are structurally similar, three key residues tailor the binding pocket to disfavor lysine binding in HalD. We therefore wondered whether expansion of the HalD binding pocket to resemble the pocket in HalB might enhance chlorination of lysine. As Trp254 appeared to have the most significant effect on the structure of the binding pocket, we cloned, expressed, and purified HalD W254F to expand the native substrate binding pocket. We next performed steady-state kinetic analyses of the wild-type and mutant halogenase enzymes with lysine and ornithine as substrates (*SI Appendix,* Figs. S16–S18). Consistent with our proposed role of the substrate binding pocket, mutagenesis of Trp254 to Phe lowered the K_M for lysine nearly 10-fold (0.13 mM) compared to wild-type HalD (1.2 mM, Fig. 6*C*). Mutagenesis also resulted in an increase in k_{cat} with lysine from 16 min^{-1} to 28 min^{-1}, suggesting that expansion of the substrate binding pocket significantly improves accommodation of the lysine. We also found that while HalD W254F had improved selectivity for lysine chlorination over hydroxylation compared to wild-type HalD, it did not fully match that of HalB (*SI Appendix,* Fig. S19).

Given that this single mutant resulted in nearly a complete switch of HalD parameters to match that of HalB, we next cloned, expressed, and purified HalD I250M I253M W254F to account for other differences in the active site in an attempt to further improve activity on lysine. While the triple mutant had slightly decreased K_M for lysine (0.45 mM), this mutant exhibited decreased k_{cat} for both ornithine and lysine suggesting that the additional mutations may destabilize the packing of the C-terminal lid onto the base of the structure, resulting in decreased rates (*SI Appendix,* Fig. S20). Taken together, these crystallographic and engineering studies suggest that mutagenesis of the C-terminal region enables engineering of amino acid halogenases with improved activity on target substrates.

Discussion

Biocatalytic C–H activation reactions take advantage of the ability of enzymes to achieve exquisite site- and stereoselectivity in the generation of a substrate radical that can undergo subsequent functionalization with a nearby group. As such, engineering this reaction class can open the door to reimagining the interface between biological and chemical catalysis with the ultimate goal of achieving the synthesis of complex molecules at low cost and

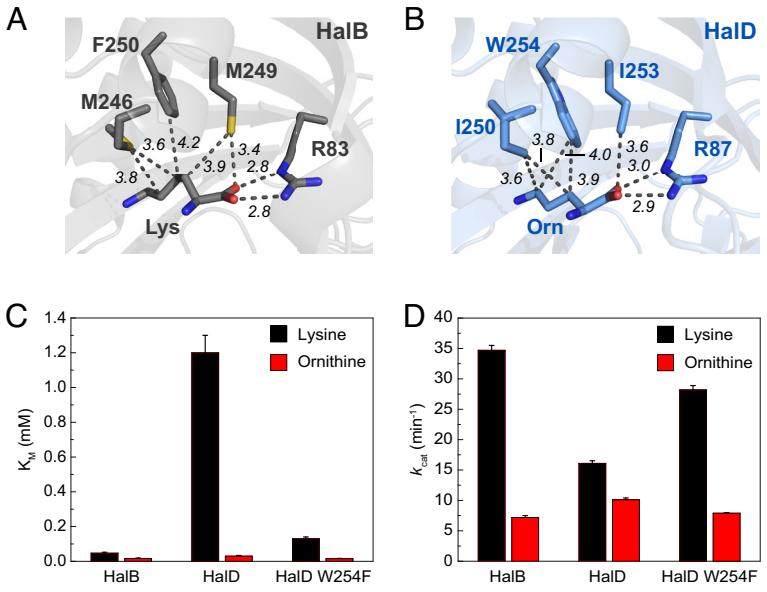

Fig. 6. Engineering altered chain length selectivity. (*A*) In the lysine halogenase, HalB, the substrate binding pocket is composed of Met246, Met249, and Phe250. (*B*) In the ornithine halogenase, HalD, the substrate binding pocket is composed of Ile250, Ile253, and Trp254. (*C* and *D*) Steady-state kinetic analysis of HalB, HalD, and HalD W254F with lysine (black) or ornithine (red) as substrates. Michaelis-Menten data are in *SI Appendix*, Figs. S15–S17 as are mean ± SD (n = 3 technical replicates). The kinetic parameters k_{cat} and K_M were calculated by nonlinear curve fitting to the Michaelis–Menten equation. Calculated K_M values are plotted as mean ± SE in panel (*C*). Calculated k_{cat} values are plotted as mean ± SE in (*D*).

environmental impact. We have focused on studying the recently discovered BesD family of amino acid halogenases, which directly chlorinate amino acids, as engineering the substrate scope of these enzymes could allow for metabolic and chemical diversification to produce an enormous range of structures.

Toward this goal, we have investigated the mechanisms by which enzymes within the BesD family evolved both site-selectivity and substrate-selectivity with respect to site selection on a methylene chain. Halogenation has particularly stringent requirements for substrate positioning, explained by the strong distance dependence for chlorination compared to the thermodynamically-preferred competing hydroxylation pathway (34, 35). Unlike hydroxylation, rebound with chloride does not take place along the same reaction vector as C–H abstraction by Fe(IV)=O, so we therefore expect that this delicate balance of substrate positioning will be important in similar atom transfer reactions. In this work, we discovered that a variable substrate-binding lid participates in an unprecedented conformational change featuring a helix-to-sheet transition upon substrate binding and is key to controlling reaction outcome. Interestingly, these lids are found in other Fe/αKG-dependent and Rieske enzymes and may play a similar role in substrate positioning in these enzymes given the shared need to close the active site and protect the substrate radical from water (53, 65, 66).

Structural and biochemical comparisons of BesD (4-Cl-lysine), HalB (5-Cl-lysine), and HalD (4-Cl-ornithine) show that divergent selectivity arises by control of the substrate conformation within the active site rather than by translational shifting. A comparison of the lysine-bound structures of HalB and BesD reveals differences in the substrate covering lids that serve to orient the substrate to achieve the desired selectivity. In particular, Met246 shapes the substrate pocket of HalB such that C_5 of lysine is most proximal to the catalytic site. Mutagenesis of Met246 to the smaller nonpolar residues Leu, Ile, and Val relieves the steric constraints and disrupts the site-selectivity, leading to halogenation at C_4. Consistent with this model, the substrate covering lid of HalD enables selectivity for the smaller, 5-carbon substrate, ornithine, over the larger 6-carbon substrate, lysine. While the covering lid of HalD is structurally similar to that of HalB, the identity of residues that form the substrate binding pocket vary. Specifically, HalD contains the larger Trp254 compared to Phe250 found in HalB and fails to accommodate lysine as effectively as it does ornithine (40-fold difference in K_M). The structure-guided expansion of the HalD active site to accommodate lysine with a K_M rivaling that of native HalB supports the role of the C-terminal lid in substrate selection and sets the stage for future engineering efforts to harness the reactivity of the iron complex for C–H activation and halogenation of nonnative substrates.

The enzymes in this study showcase the tremendous power of biocatalysis. This work provides fundamental insights into how BesD, HalB, and HalD use the same catalytic metal center to perform subtly different reactions with high selectivity. In addition to chlorination, enzymes in this family have been shown to perform bromination and azidation, further illustrating the versatility of these enzymes for biocatalysis. (51) The application and evolution of radical halogenases toward modification of C–H bonds have the potential to bridge biological and chemical methods for bond formation, broadening the scope of accessible compounds.

Materials and Methods

Detailed *Materials and Methods* are described in the *SI Appendix*.

Protein Plasmid Generation, Expression, and Purification. Templates were obtained as synthetic genes and expression plasmids were produced by Gibson assembly into NdeI/BamHI digested pET16b in *Escherichia coli* DH10B-T1^R. Protein expression was carried out in *E. coli* BL21 Star (DE3) harboring the pRARE2 plasmid by induction with 0.25 mM IPTG for 20 h at 16 °C. Protein was purified using Ni-NTA agarose before buffer exchange into storage buffer and storage at −80 °C. Protein for crystallography was further purified by anion exchange and size exclusion chromatography.

Protein Crystallization and Data Collection. Crystals were obtained by the hanging drop vapor diffusion method combining equal volumes of protein solution and reservoir solution. Crystals were flash frozen in liquid nitrogen and data

was collected at Beamline 8.3.1 at the Advanced Light Source at a wavelength of 1.11 Å. Data were processed using X-ray detector software (XDS) and phased using the structure of BesD (6NIE) as a search model. The structures were iteratively refined in COOT and Phenix.

Fluorogenic Screen to Detect 4-Cl-Lysine Production. Chemically competent *E. coli* BL21 cells harboring the pBesBC plasmid were transformed with SwHalB NNK libraries. Colonies were expressed overnight before dilution into M9 media supplemented with lysine. After 4 d of expression at 16 °C, the cells were pelleted by centrifugation and media samples were transferred to 96 well plates containing a CuAAC reaction mixture. After 30 min of reaction, the plates were analyzed for the presence of the Pra-CalFluor product (λ_{ex} = 485 nm, λ_{em} = 528 nm) using a SynergyMx Microplate Reader (BioTek) at room temperature.

Kinetic Analysis of Enzyme Variants. Steady-state kinetic analysis was performed by monitoring NADH consumption through a coupled assay dependent on succinate production resulting from enzyme turnover. Reactions were initiated through the addition of the halogenase variant to various concentrations of substrate. Initial rates of NADH consumption were measured by monitoring A_{340} at room temperature. Kinetic parameters were determined from fitting of the initial rate data to the Michaelis–Menten equation.

In Vitro Assays of Halogenase Variants. Reactions were initiated by the addition of purified enzyme to a mixture containing substrate, αKG, iron, and sodium ascorbate at room temperature. After 25 min, reactions were quenched by addition of 2 vol of methanol with 1% (*v/v*) formic acid. Samples were analyzed by LC/MS using a SeQuant ZIC-pHILIC on an Agilent 1290 UPLC-QTOF in positive ionization mode.

Data, Materials, and Software Availability. X-ray structure data has been deposited in the PDB (7U6I, 7U6J, 7U6H) (67–69). All study data are included in the article and/or *SI Appendix*.

ACKNOWLEDGMENTS. This work was funded by generous support from the NIH (R01 GM134271). E.N.K. acknowledges the support of a NIH National Research Service Award Training Grant (1 T32 GMO66698). M.E.N. acknowledges the support of a NSF Graduate Research Fellowship. C.V.S. acknowledges the support of a Berkeley Fellowship for Graduate Study. J.A.M. acknowledges the support of a UC Berkeley Chancellor's Fellowship, Howard Hughes Medical Institute Gilliam Fellowship, and NIH NRSA Training Grant (1 T32 GMO66698). X-ray data were collected at the Advanced Light Source Beamline 8.3.1, which is operated by the University of California Office of the President, Multicampus Research Programs and Initiatives (MR-15-328599), the NIH (R01 GM124149 and P30 GM124169), Plexxikon Inc., and the Integrated Diffraction Analysis Technologies program of the U.S. Department of Energy Office of Biological and Environmental Research. The Advanced Light Source is a national user facility operated by Lawrence Berkeley National Laboratory on behalf of the U.S. Department of Energy under contract number DEAC02-05CH11231, Office of Basic Energy Sciences. We thank Dr. Hasan Celik and UC Berkeley's NMR facility in the College of Chemistry (CoC-NMR) for spectroscopic assistance. Instruments in the CoC-NMR are supported in part by NIH S10OD024998. We also acknowledge Max Sosa and Dr. Elizabeth Stone for their generous assistance in interpreting NMR spectra.

Author affiliations: [a]Department of Chemistry, University of California, Berkeley, CA 94720; [b]Department of Chemical and Biomolecular Engineering, University of California, Berkeley, CA 94720; and [c]Department of Molecular and Cell Biology, University of California, Berkeley, CA 94720

1. F. Rudroff *et al.*, Opportunities and challenges for combining chemo- and biocatalysis. *Nat. Catal.* **1**, 12–22 (2018).
2. P. N. Devine *et al.*, Extending the application of biocatalysis to meet the challenges of drug development. *Nat. Rev. Chem.* **2**, 409–421 (2018).
3. C. K. Savile *et al.*, Biocatalytic asymmetric synthesis of chiral amines from ketones applied to sitagliptin manufacture. *Science* **329**, 305–309 (2010).
4. M. A. Huffman *et al.*, Design of an in vitro biocatalytic cascade for the manufacture of islatravir. *Science* **366**, 1255–1259 (2019).
5. C. M. Clouthier, J. N. Pelletier, Expanding the organic toolbox: A guide to integrating biocatalysis in synthesis. *Chem. Soc. Rev.* **41**, 1585–1605 (2012).
6. E. J. Craven *et al.*, Programmable late-stage C−H bond functionalization enabled by integration of enzymes with chemocatalysis. *Nat. Catal.* **4**, 385–394 (2021).
7. L. J. Durak, J. T. Payne, J. C. Lewis, Late-stage diversification of biologically active molecules via chemoenzymatic C-H functionalization. *ACS Catal.* **6**, 1451–1454 (2016).
8. J. B. Pyser, S. Chakrabarty, E. O. Romero, A. R. H. Narayan, State-of-the-art biocatalysis. *ACS Cent. Sci.* **7**, 1105–1116 (2021).
9. G. Meng *et al.*, Achieving site-selectivity for C-H activation processes based on distance and geometry: A carpenter's approach. *J. Am. Chem. Soc.* **142**, 10571–10591 (2020).
10. N. Y. S. Lam *et al.*, Empirical guidelines for the development of remote directing templates through quantitative and experimental analyses. *J. Am. Chem. Soc.* **144**, 2793–2803 (2022).
11. T. Zhang *et al.*, A directive Ni catalyst overrides conventional site selectivity in pyridine C-H alkenylation. *Nat. Chem.* **13**, 1207–1213 (2021).
12. M. I. Gonzalez *et al.*, Taming the chlorine radical: Enforcing steric control over chlorine-radical-mediated C-H activation. *J. Am. Chem. Soc.* **144**, 1464–1472 (2022).
13. J. He, M. Wasa, K. S. L. Chan, Q. Shao, J.-Q. Yu, Palladium-catalyzed transformations of alkyl C-H bonds. *Chem. Rev.* **117**, 8754–8786 (2017).
14. T. W. Lyons, M. S. Sanford, Palladium-catalyzed ligand-directed C−H functionalization reactions. *Chem. Rev.* **110**, 1147–1169 (2010).
15. R. Oeschger *et al.*, Diverse functionalization of strong alkyl C-H bonds by undirected borylation. *Science* **368**, 736–741 (2020).
16. S. P. Ross, A. A. Rahman, M. S. Sigman, Development and mechanistic interrogation of interrupted chain-walking in the enantioselective relay heck reaction. *J. Am. Chem. Soc.* **142**, 10516–10525 (2020).
17. J. Zhang, X. Huang, R. K. Zhang, F. H. Arnold, Enantiodivergent α-amino C-H fluoroalkylation catalyzed by engineered cytochrome P450s. *J. Am. Chem. Soc.* **141**, 9798–9802 (2019).
18. L. E. Zetzsche *et al.*, Biocatalytic oxidative cross-coupling reactions for biaryl bond formation. *Nature* **603**, 79–85 (2022).
19. C. K. Prier, R. K. Zhang, A. R. Buller, S. Brinkmann-Chen, F. H. Arnold, Enantioselective, intermolecular benzylic C-H amination catalysed by an engineered iron-haem enzyme. *Nat. Chem.* **9**, 629–634 (2017).
20. M. L. Matthews *et al.*, Direct nitration and azidation of aliphatic carbons by an iron-dependent halogenase. *Nat. Chem. Biol.* **10**, 209–215 (2014).
21. S. B. J. Kan, R. D. Lewis, K. Chen, F. H. Arnold, Directed evolution of cytochrome c for carbon-silicon bond formation: Bringing silicon to life. *Science* **354**, 1048–1051 (2016).
22. S. B. J. Kan, X. Huang, Y. Gumulya, K. Chen, F. H. Arnold, Genetically programmed chiral organoborane synthesis. *Nature* **552**, 132–136 (2017).
23. R. K. Zhang, X. Huang, F. H. Arnold, Selective CH bond functionalization with engineered heme proteins: New tools to generate complexity. *Curr. Opin. Chem. Biol.* **49**, 67–75 (2019).
24. F. Li, H. Renata, A chiral-pool-based strategy to access trans-syn-fused drimane meroterpenoids: Chemoenzymatic total syntheses of polysin, N-acetyl-polyveoline and the chrodrimanins. *J. Am. Chem. Soc.* **143**, 18280–18286 (2021).
25. X. Zhang *et al.*, Divergent synthesis of complex diterpenes through a hybrid oxidative approach. *Science* **369**, 799–806 (2020).
26. A. Amatuni, A. Shuster, A. Adibekian, H. Renata, Concise chemoenzymatic total synthesis and identification of cellular targets of cepafungin I. *Cell Chem. Biol.* **27**, 1318–1326.e18 (2020).
27. D. S. Gkotsi, J. Dhaliwal, M. M. McLachlan, K. R. Mulholand, R. J. Goss, Halogenases: Powerful tools for biocatalysis (mechanisms applications and scope). *Curr. Opin. Chem. Biol.* **43**, 119–126 (2018).
28. L. C. Blasiak, F. H. Vaillancourt, C. T. Walsh, C. L. Drennan, Crystal structure of the non-haem iron halogenase SyrB2 in syringomycin biosynthesis. *Nature* **440**, 368–371 (2006).
29. J. M. Bollinger, "CHAPTER 3: Mechanisms of 2-oxoglutarate-dependent oxygenases: The hydroxylation paradigm and beyond" in *2-Oxoglutarate-Dependent Oxygenases* (Royal Society of Chemistry, 2015), pp. 95–122.
30. J. Büchler *et al.*, Algorithm-aided engineering of aliphatic halogenase WelO5* for the asymmetric late-stage functionalization of soraphens. *Nat. Commun.* **13**, 371 (2022).
31. A. L. Lukowski, J. Liu, J. Bridwell-Rabb, A. R. H. Narayan, Structural basis for divergent C-H hydroxylation selectivity in two Rieske oxygenases. *Nat. Commun.* **11**, 2991 (2020).
32. J. Liu *et al.*, Design principles for site-selective hydroxylation by a Rieske oxygenase. *Nat. Commun.* **13**, 255 (2022).
33. J. Stubbe, W. A. van der Donk, Protein radicals in enzyme catalysis. [Chem. Rev. 1998, 98, 705−762.] *Chem. Rev.* **98**, 2661–2662 (1998).
34. S. D. Wong *et al.*, Elucidation of the Fe(IV)=O intermediate in the catalytic cycle of the halogenase SyrB2. *Nature* **499**, 320–323 (2013).
35. M. Srnec, E. I. Solomon, Frontier molecular orbital contributions to chlorination versus hydroxylation selectivity in the non-heme iron halogenase SyrB2. *J. Am. Chem. Soc.* **139**, 2396–2407 (2017).
36. A. J. Mitchell *et al.*, Structural basis for halogenation by iron- and 2-oxo-glutarate-dependent enzyme WelO5. *Nat. Chem. Biol.* **12**, 636–640 (2016).
37. R. J. Martinie *et al.*, Experimental correlation of substrate position with reaction outcome in the aliphatic halogenase, SyrB2. *J. Am. Chem. Soc.* **137**, 6912–6919 (2015).
38. V. Agarwal *et al.*, Enzymatic halogenation and dehalogenation reactions: Pervasive and mechanistically diverse. *Chem. Rev.* **117**, 5619–5674 (2017).
39. F. H. Vaillancourt, E. Yeh, D. A. Vosburg, S. E. O'Connor, C. T. Walsh, Cryptic chlorination by a non-haem iron enzyme during cyclopropyl amino acid biosynthesis. *Nature* **436**, 1191–1194 (2005).
40. D. P. Galonić, F. H. Vaillancourt, C. T. Walsh, Halogenation of unactivated carbon centers in natural product biosynthesis: Trichlorination of leucine during barbamide biosynthesis. *J. Am. Chem. Soc.* **128**, 3900–3901 (2006).
41. M. Ueki *et al.*, Enzymatic generation of the antimetabolite gamma, gamma-dichloroaminobutyrate by NRPS and mononuclear iron halogenase action in a streptomycete. *Chem. Biol.* **13**, 1183–1191 (2006).
42. C. S. Neumann, C. T. Walsh, Biosynthesis of (-)-(1S,2R)-allocoronamic acyl thioester by an Fe(II)-dependent halogenase and a cyclopropane-forming flavoprotein. *J. Am. Chem. Soc.* **130**, 14022–14023 (2008).
43. S. M. Pratter *et al.*, More than just a halogenase: Modification of fatty acyl moieties by a trifunctional metal enzyme. *Chembiochem Eur. J. Chem. Biol.* **15**, 567–574 (2014).
44. W. Jiang *et al.*, Biosynthetic chlorination of the piperazate residue in kutzneride biosynthesis by KthP. *Biochemistry* **50**, 6063–6072 (2011).

45. P. M. Flatt *et al.*, Characterization of the initial enzymatic steps of barbamide biosynthesis. *J. Nat. Prod.* **69**, 938–944 (2006).
46. D. Khare *et al.*, Conformational switch triggered by alpha-ketoglutarate in a halogenase of curacin A biosynthesis. *Proc. Natl. Acad. Sci. U.S.A.* **107**, 14099–14104 (2010).
47. M. L. Hillwig, X. Liu, A new family of iron-dependent halogenases acts on freestanding substrates. *Nat. Chem. Biol.* **10**, 921–923 (2014).
48. C. Zhao *et al.*, An Fe2+ - and α-ketoglutarate-dependent halogenase acts on nucleotide substrates. *Angew. Chem. Int. Ed. Engl.* **59**, 9478–9484 (2020).
49. J. A. Marchand *et al.*, Discovery of a pathway for terminal-alkyne amino acid biosynthesis. *Nature* **567**, 420–424 (2019).
50. M. L. Hillwig, Q. Zhu, K. Ittiamornkul, X. Liu, Discovery of a promiscuous non-heme iron halogenase in ambiguine alkaloid biogenesis: Implication for an evolvable enzyme family for late-stage halogenation of aliphatic carbons in small molecules. *Angew. Chem. Int. Ed. Engl.* **55**, 5780–5784 (2016).
51. M. E. Neugebauer *et al.*, A family of radical halogenases for the engineering of amino-acid-based products. *Nat. Chem. Biol.* **15**, 1009–1016 (2019).
52. M. A. T. Blaskovich, Unusual amino acids in medicinal chemistry. *J. Med. Chem.* **59**, 10807–10836 (2016).
53. K. Bastard, T. Isabet, E. A. Stura, P. Legrand, A. Zaparucha, Structural studies based on two lysine dioxygenases with distinct regioselectivity brings insights into enzyme specificity within the clavaminate synthase-like family. *Sci. Rep.* **8**, 16587 (2018).
54. R. P. Hausinger, "CHAPTER 1: Biochemical diversity of 2-oxoglutarate-dependent oxygenases" in *2-Oxoglutarate-Dependent Oxygenases* (Royal Society of Chemistry, 2015), pp. 1–58.
55. M. L. Matthews *et al.*, Substrate positioning controls the partition between halogenation and hydroxylation in the aliphatic halogenase, SyrB2. *Proc. Natl. Acad. Sci. U.S.A.* **106**, 17723–17728 (2009).
56. R. Mehmood, V. Vennelakanti, H. J. Kulik, Spectroscopically guided simulations reveal distinct strategies for positioning substrates to achieve selectivity in nonheme Fe(II)/α-ketoglutarate-dependent halogenases. *ACS Catal.* **11**, 12394–12408 (2021).
57. H. Renata, E. Shimizu, C. R. Zwick, Regiodivergent biocatalytic hydroxylation of L-glutamine facilitated by characterization of non-heme dioxygenases from non-ribosomal peptide biosyntheses. *Tetrahedron* **90**, 132190 (2021).
58. I. J. Clifton, L. C. Hsueh, J. E. Baldwin, K. Harlos, C. J. Schofield, Structure of proline 3-hydroxylase. Evolution of the family of 2-oxoglutarate dependent oxygenases. *Eur. J. Biochem.* **268**, 6625–6636 (2001).
59. H. Mori, T. Shibasaki, Y. Uozaki, K. Ochiai, A. Ozaki, Detection of novel proline 3-hydroxylase activities in streptomyces and bacillus spp. by regio- and stereospecific hydroxylation of l-Proline. *Appl. Environ. Microbiol.* **62**, 1903–1907 (1996).
60. M. E. Neugebauer *et al.*, Reaction pathway engineering converts a radical hydroxylase into a halogenase. *Nat. Chem. Biol.* **18**, 171–179 (2022).
61. P. Shieh *et al.*, CalFluors: A universal motif for fluorogenic azide probes across the visible spectrum. *J. Am. Chem. Soc.* **137**, 7145–7151 (2015).
62. L. Luo *et al.*, An assay for Fe(II)/2-oxoglutarate-dependent dioxygenases by enzyme-coupled detection of succinate formation. *Anal. Biochem.* **353**, 69–74 (2006).
63. A. C. Guo *et al.*, ECMDB: The E. coli metabolome database. *Nucleic Acids Res.* **41**, D625–630 (2013).
64. M. G. Thompson *et al.*, An iron (II) dependent oxygenase performs the last missing step of plant lysine catabolism. *Nat. Commun.* **11**, 2931 (2020).
65. Y. Ashikawa *et al.*, Electron transfer complex formation between oxygenase and ferredoxin components in Rieske nonheme iron oxygenase system. *Structure* **14**, 1779–1789 (2006).
66. Y. Ashikawa *et al.*, Structural insight into the substrate- and dioxygen-binding manner in the catalytic cycle of rieske nonheme iron oxygenase system, carbazole 1,9a-dioxygenase. *BMC Struct. Biol.* **12**, 15 (2012).
67. M. E. Neugebauer, E. N. Kissman, M. C. Y. Chang, HalB with glycine and succinate. Protein Data bank. https://www.rcsb.org/structure/7U6I. Deposited 4 March 2022.
68. K. S. Sumida, M. E. Neugebauer, E. N. Kissman, M. C. Y. Chang, HalB with lysine and succinate. Protein Data Bank. https://www.rcsb.org/structure/7U6J. Deposited 4 March 2022.
69. C. V. Swenson, M. E. Neugebauer, E. N. Kissman, M. C. Y. Chang, HalD with ornithine and alpha-ketoglutarate. Protein Data Bank. https://www.rcsb.org/structure/7U6H. Deposited 4 March 2022.